Modeling and observer design for aluminum manufacturing

Lucas José da Silva Moreira, Mirko Fiacchini, Gildas Besançon, Francesco Ferrante, Hervé Roustan

Modeling and Observer Design for Aluminum Manufacturing ⋆

Lucas José da Silva Moreira[a], Mirko Fiacchini[a], Gildas Besançon[a], Francesco Ferrante[b], Hervé Roustan[c]

[a] *Univ. Grenoble Alpes, CNRS, Grenoble INP, GIPSA-lab, Grenoble, France. (e-mail: lucas-jose.da-silva-moreira, mirko.fiacchini , gildas.besancon @grenoble-inp.fr).*
[b] *Department of Engineering, University of Perugia, Via G. Duranti, 67, 06125 Perugia, Italy, (email: francesco.ferrante@unipg.it)*
[c] *Rio Tinto, Laboratoire de Recherche des Fabrications, Saint Jean de Maurienne, France(e-mail: herve.roustan@riotinto.com)*

Abstract

This paper addresses modeling, identification, and observer design of the Hall-Héroult process. This process is the main core of aluminum manufacturing. More specifically, by building upon a blend of physical-chemical constitutive relations and system identification tools, this paper first provides a model describing the interplay of Anode-Cathode Distance (ACD), alumina concentration, and pot pseudo-resistance. The proposed model is then used to tune a linear Kalman filter generating online estimates of the plant state variables. The proposed approach is validated via data taken from a real industrial plant.

Keywords: physical modeling, parameter identification, observer design, Kalman Filter, industrial application

1. Introduction

Aluminum is produced in large scale via the Hall-Heroult electrolysis process since the 19th century [1]. This process is carried out by dipping carbon anodes into a cryolite bath solution that contains dissolved alumina (Al_2O_3). A high intensity electric current is applied to the system and the chemical process produces liquid aluminum cumulating at the bottom of the cell, and releases

⋆This research was partially supported by project FUI-AAP 25 PIANO.

carbon dioxide. The process is summarized by the following chemical reaction:

$$Al_2O_{3(diss)} + \frac{3}{2}C_{(anode)} \rightarrow 2Al_{(l)} + \frac{3}{2}CO_{2(g)} \quad (1)$$

A schematic representation of a simple pot cell is shown in Figure 1. To enhance production, industrial plants have a large number of anodes connected in parallel by a common bar for each electrolysis cell. The height of this bar can be adjusted to change the Anode-Cathode Distance (ACD). This distance is not constant during the operation due to the chemical reaction. Indeed, the carbon anodes are consumed and they are replaced after some time, while the liquid aluminum layer increases because of the production. Furthermore, perturbations of the current and bath composition can affect the ACD. However, the hazardous conditions inside the pot make it impossible to develop a sensor for continuous measurement of the system state. The ACD value is critical since a large distance decreases the pot cell efficiency and a small value can cause a short-circuit between the produced aluminum and the anode [2, 3]. A recent study shows that an effective ACD regulation can improve cell energy consumption [4] and consequently increase the efficiency as shown in [5]. Unfortunately, the mechanisms behind this process are complex and only a few papers have modeled this dynamical behavior in detail [6, 7].

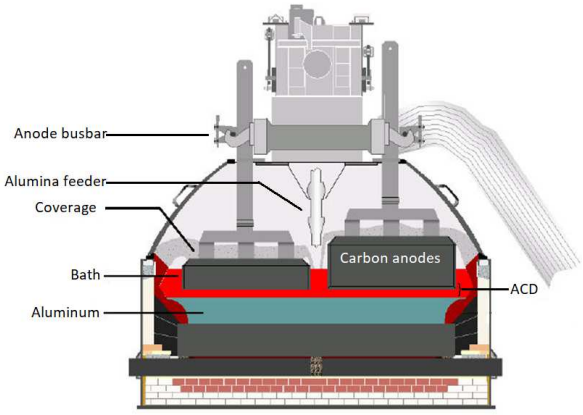

Figure 1: Pot Schematic View

The dissolved alumina concentration (wAl_2O_3) is also an important quantity that is not continuously measured. Usually, alumina is injected in powder state by individual feeders distributed along the cell according to a predefined sequence. Low values of alumina concentration can cause the so-called *anode effect*, a deleterious phenomenon leading to the production of greenhouse gases [8]. However, a large alumina powder injection does not induce an instantaneous change in the concentration and it can possibly produce sludge phenomena. This is an undesired condition since the accumulation of undissolved alumina in the bath can lead to cell damages [9]. Commonly, just a few measurements of the alumina concentration per week are manually taken, which makes it difficult to obtain an experimental model.

In actual plants, only the line current applied to the system (I), the pot cell voltage (V), the busbar motion (BM), and the frequency of the alumina feeding (F) are continuously collected by sensors. For the system regulation, an indirect measurement called "pseudo-resistance" (R) is commonly used to adjust ACD and wAl_2O_3. Based on the pseudo-resistance value, the alumina feeding frequency is modified, alternating between two pre-determined periods to have faster or slower feeding [7]. Moreover, the pseudo-resistance is adjusted via the ACD regulation to ensure system stability and obtain a good current efficiency [10]. From this complex relation, it is not easy to obtain information about the instantaneous values of ACD and wAl_2O_3. Therefore, it is important to model this process to be able to generate online estimations for those quantities.

Some researchers have been developing nonlinear estimators to overcome this information limitation and obtain the desired process states [11, 6, 12]. However, those works are mostly based on the *Extended* Kalman Filter [13], i.e. on approximate model linearization on the one hand (facing all related drawbacks), and do not rely much on the underlying physics of the process on the other hand.

In this context, and on the basis of a plant in actual industrial operation, the present paper proposes a modeling methodology for Hall-Héroult process, which enables real time estimation of ACD and wAl_2O_3, as an extension of our pre-

liminary works of [14, 15]. Despite its simplicity, our model captures the main features of regular operations conditions by combining physical-chemical aspects with experimental models. Furthermore, in spite of its nonlinearity, we show how tools from *linear* systems theory can be used by separating the estimation problem in two steps: identification in a first one, with least square optimization, and state observer design in a second one, via an appropriate rewriting and an exact linear Kalman Filter approach (referring to formal results of [16] for instance). Finally, the proposed method is validated on industrial data, taken in actual operational conditions. This paper extends our previous work in multiple directions [14, 15]:

First, the ACD physical model is here explained in details by a chemical balance analysis.

Additionally, a simplification in the alumina concentration is done by avoiding any time delay. This is reasonable since the available alumina measurements have been taken at intervals of several hours.

Moreover, the alumina dissolving dynamics has a time response of several minutes. Thus, a delay of one minute, or even slightly more, is not expected to relevantly affect the value of the alumina at the measurement instants and then a relatively accurate alumina model can be identified even by neglecting the delay.

Furthermore, the pot pseudo-resistance is represented by a specific polynomial function with new identification procedure.

Finally, validation tests are carried out with new sets of data to ensure robustness, collected from industrial APXe pot cell of Rio Tinto Laboratoire des Recherches de Fabrications (LRF) located in Saint Jean de Maurienne, France, in regular operation. The data used in this paper was collected during daily industrial operations. Therefore, all the parameters identification and state estimation procedures are performed with real signals that are generated aiming at operation safety and production goals. Notice that for confidentiality reasons, the data details in the y-axis of all plots and the values of the estimated coefficients are not shown.

The paper is organized as follows: Section 2 presents the proposed physical-based modeling equations, and Section 3 discusses the related identification approach. Section 4 shows the use of this model for state estimation. The conclusions are presented in Section 5.

2. Modeling

The complex electrochemical process under consideration is modeled in discrete-time since the goal is a real-time application of Linear Kalman Filter tools. It is aimed to capture the average dynamics of the pot cell. Hence, the respective states represent global indicators of the plant. This means that local conditions such as the current distribution and anode change effect are not taken into account explicitly. In this context, the models of the unmeasured quantities ACD and wAl_2O_3 are related to the available inputs, i.e. beam motion and frequency of feeders, as well as the measured disturbance of the electric line current. Then, the system output, i.e. the pseudo-resistance, is related to the modeled states. The model is obtained using a hybrid approach that combines physical-chemical aspects and information extracted from data. Moreover, the sampling time of 1 minute is selected because the time constant for the dissolution of alumina is in this order of magnitude and to avoid the noise influence [17].

2.1. Anode-Cathode Distance

From the problem description, it is possible to define the derivative of the ACD ($\frac{d}{dt}ACD$) as a result of the height variations of the aluminum ($\frac{d}{dt}Al_{height}$), the carbon ($\frac{d}{dt}C_{height}$) layer, and the anodes busbar beam position ($\frac{d}{dt}BM$):

$$\frac{d}{dt}ACD = \frac{d}{dt}Al_{height} - \frac{d}{dt}C_{height} + \frac{d}{dt}BM \tag{2}$$

Each layer height can be written as a function of the mass production using the corresponding densities. Hence, the aluminum and carbon height variations become:

$$\frac{d}{dt}Al_{height} = \frac{1}{\rho_{Al}S}\left[\frac{d}{dt}m_{Al}\right] \tag{3}$$

$$\frac{d}{dt}C_{height} = \frac{1}{\rho_C S}\left[\frac{d}{dt}m_C\right] \tag{4}$$

where ρ_{Al} is the liquid aluminum density, m_{Al} is the aluminum produced mass, ρ_C is the carbon density, m_C is the carbon produced mass, and S is the average reaction surface area.

The produced aluminum mass rate ($\frac{d}{dt}m_{Al}$) is given by Faraday's law of electrolysis [18]:

$$\frac{d}{dt}m_{Al} = \frac{C_e Al_m}{3\mathfrak{F}} I \tag{5}$$

where C_e is the current efficiency, Al_m is the aluminum molar mass, I is the line current, $\mathfrak{F}$ is the Faraday's constant, and 3 corresponds to the valency number of aluminum ions obtained via the following reaction:

$$4Al^{3+} + 6O^{2-} + 3C_{(anode)} \rightarrow 4Al_{(l)} + 3CO_{2(g)} \tag{6}$$

From the chemical balance in (1), it is possible to relate the aluminum mass production with the carbon mass consumption. This leads to the following expression for the carbon mass consumption rate $\frac{d}{dt}m_C$:

$$\frac{d}{dt}m_C = \frac{C_m}{4\mathfrak{F}} I \tag{7}$$

where C_m is the carbon molar mass and 4 is the stoichiometric coefficient.

Hence, equation (2) can be rewritten using the above expressions as:

$$\frac{d}{dt}ACD = \frac{1}{S\mathfrak{F}}\left(\frac{C_e Al_m}{3\rho_{Al}} - \frac{C_m}{4\rho_C}\right) I + \frac{d}{dt}BM \tag{8}$$

The beam position variation is considered as one of the system inputs (U_1):

$$U_1 := \frac{d}{dt}BM \tag{9}$$

Hence, by defining β as:

$$\beta := \frac{1}{S\mathfrak{F}}\left(\frac{C_e Al_m}{3\rho_{Al}} - \frac{C_m}{4\rho_C}\right) \tag{10}$$

and using equation (10) in (8), the ACD dynamics result as:

$$\frac{d}{dt}ACD = \beta I + U_1 \tag{11}$$

In discrete-time, equation (11) becomes:

$$ACD[n+1] = ACD[n] + \beta i[n] + u_1[n] \tag{12}$$

$ACD[n]$ stands for $ACD(nT_s)$ for a sampling time T_s, i and u_1 are discretized integrals of I and U_1 respectively over T_s with N_s samples, as:

$$u_1[n] = \sum_{k=1}^{N_s} U_1\left(\left(\frac{k}{N_s} + n\right) T_s\right) \tag{13}$$

$$i[n] = \sum_{k=1}^{N_s} I\left(\left(\frac{k}{N_s} + n\right) T_s\right) \tag{14}$$

Remark 1. As it is not possible to measure the ACD during the operation of the plant, β cannot be obtained experimentally. Hence, this parameter is calculated using theoretical values for a regular pot operation.

2.2. Alumina Concentration

The variation of the alumina concentration wAl_2O_3 can be modeled as the difference between the quantity injected by the feeders (wAl_2O_{3in}) and the one consumed by the chemical reaction (wAl_2O_{3cons}):

$$\frac{d}{dt} wAl_2O_3 = wAl_2O_{3in} - wAl_2O_{3cons} \tag{15}$$

The quantity injected by the feeders at time t can be represented by:

$$wAl_2O_{3in} = \frac{N_g m_{in}}{M} F \tag{16}$$

where N_g is the number of feeders in the pot, m_{in} is the amount of mass injected by feeders, M is the total bath mass, and F is the frequency of feeders. As the sampling time for this process is typically large, we assume that the alumina dissolving dynamics can be neglected.

The frequency of the feeders is considered as a second system input:

$$U_2 := F \tag{17}$$

Then, equation (16) becomes:

$$wAl_2O_{3in} = \frac{N_g m_{in}}{M} U_2 \tag{18}$$

The Al_2O_3 consumption is given by the Faraday's law divided by the bath mass:

$$wAl_2O_{3cons} = \frac{Al_2O_{3m} C_e}{6\mathfrak{F}M} I \tag{19}$$

where Al_2O_{3m} is the alumina molar mass and 6 is the number of electrons required for the electrolysis to perform. Replacing equations (18) and (19) into (15):

$$\frac{d}{dt} wAl_2O_3 = \frac{N_g m_{in}}{M} U_2 - \frac{Al_2O_{3m} C_e}{6\mathfrak{F}M} I \tag{20}$$

and defining:

$$\alpha_1 = \tfrac{N_g m_{in}}{M}, \quad \alpha_2 = \tfrac{Al_2O_{3m} C_e}{6\mathfrak{F}M} \tag{21}$$

equation (20) can be written as:

$$\frac{d}{dt} wAl_2O_3 = \alpha_1 U_2 - \alpha_2 I \tag{22}$$

A discrete-time model for wAl_2O_3 can then be obtained using a similar procedure for ACD:

$$wAl_2O_3[n+1] = wAl_2O_3[n] + \alpha_1 u_2[n] - \alpha_2 i[n] \tag{23}$$

with same notations as before, and:

$$u_2[n] = \sum_{k=1}^{N_s} U_2 \left(\left(\frac{k}{N_s} + n \right) T_s \right) \tag{24}$$

2.3. Pseudo-Resistance

Now that ACD and wAl_2O_3 models are available, it is necessary to relate them with the output signal, pseudo-resistance R. From the physical modeling described in [19], it is possible to plot a curve that relates ACD, wAl_2O_3 and R as shown in Figure 2.

However, this relation is complex and takes into account other quantities that cannot be continuously measured. One possible solution to directly relate ACD

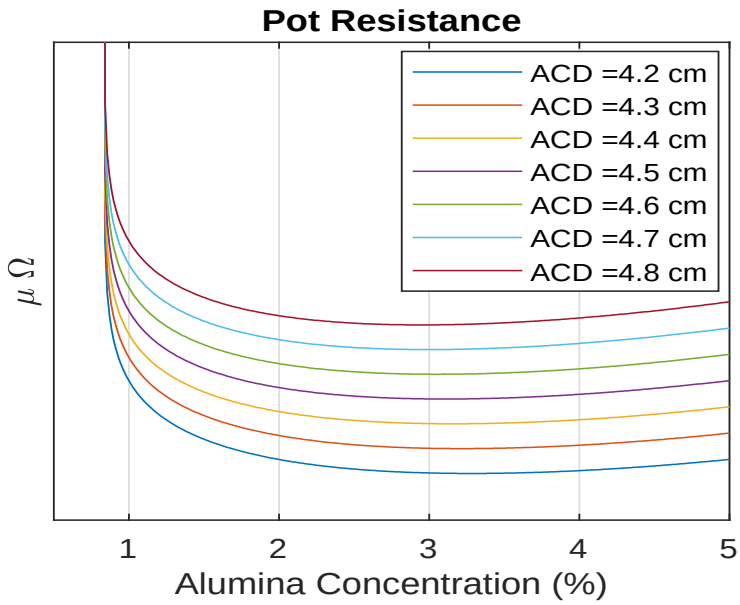

Figure 2: Typical pot resistance curve as a function of alumina concentration and ACD

and wAl_2O_3 is to approximate the curve with a polynomial function around the desired operational range. In particular, by denoting the ACD as z_1, wAl_2O_3 as z_2 and considering an alumina concentration range between 2% and 4%, the curve can be approximated as follows:

$$R = c(z_2)^2 + (d + ez_1)z_2 + (f + gz_1) \tag{25}$$

where c, d, e, f, and g are constant parameters to be determined. By differentiating equation (25), parameter f disappears and it is possible to obtain a dynamical model for the variation of pseudo-resistance as:

$$\frac{d}{dt}R = ez_1\frac{d}{dt}z_2 + \left(2c\frac{d}{dt}z_2 + e\frac{d}{dt}z_1\right)z_2 + d\frac{d}{dt}z_2 + g\frac{d}{dt}z_1 \tag{26}$$

From equations (11) and (22), the pseudo-resistance as a function of the available inputs is given by:

$$\frac{d}{dt}R = ez_1\left(\alpha_1 u_2 - \alpha_2 i\right) + \left[2c\left(\alpha_1 u_2 - \alpha_2 i\right) + e\left(\beta i + u_1\right)\right] z_2 + d\left(\alpha_1 u_2 - \alpha_2 i\right) + g\left(\beta i + u_1\right) \quad (27)$$

Using the discretization method described in previous subsections, it is possible to obtain the following model for the resistance variations:

$$R[n+1] = R[n] + e\Delta z_2[n] z_1[n] + (2c\Delta z_2[n] + e\Delta z_1[n]) z_2[n] + d\Delta z_2[n] + g\Delta z_1[n] \quad (28)$$

where:

$$\Delta z_1[n] := u_1[n] + \beta i[n] \quad (29)$$

$$\Delta z_2[n] := \alpha_1 u_2[n] - \alpha_2 i[n] \quad (30)$$

3. Identification

Using the data collected from daily operational conditions, it is possible to identify parameters α_1 and α_2 in wAl_2O_3 model equation (23). Then, the estimation can be performed for parameters c, d, e and g for R model equation (28). Next, it is presented an identification procedure, along with the corresponding validation.

3.1. Alumina Concentration

During an operational day, just few alumina concentration measurements are recorded, and without constant sampling time. Hence, to identify parameters α_1 and α_2, using the data collected at N_a times $\begin{bmatrix} n_1 T_s & n_1 T_s & \cdots & n_{N_a} T_s \end{bmatrix}$ in seconds, equation (23) can be arranged in matrix form using the accumulation

of u_2 and i signals in these intervals, as follows:

$$\begin{bmatrix} wAl_2O_3[n_2] - wAl_2O_3[n_1] \\ wAl_2O_3[n_3] - wAl_2O_3[n_2] \\ \vdots \\ wAl_2O_3[n_N] - wAl_2O_3[n_{N-1}] \end{bmatrix} = \begin{bmatrix} \sum_{k=n_1}^{n_2-1} u_2[k] & -\sum_{k=n_1}^{n_2-1} i[k] \\ \sum_{k=n_2}^{n_3-1} u_2[k] & -\sum_{k=n_2}^{n_3-1} i[k] \\ \vdots & \vdots \\ \sum_{k=n_{N-1}}^{n_N-1} u_2[k] & -\sum_{k=n_{N-1}}^{n_N-1} i[k] \end{bmatrix} \begin{bmatrix} \alpha_1 \\ \alpha_2 \end{bmatrix} \tag{31}$$

Based on the structure of equation (31), it is possible to perform a least square estimation for parameters α_1 and α_2. The experimental model is validated by a comparison between the simulated values of alumina concentration with estimated parameters and the alumina concentration values collected on the plant. Notice that the data used for validation are different from those used for the identification. The model is initialized with a real measurement. For every new alumina concentration sample collected, the model is reinitialized to improve the accuracy.

Figure 3 shows first the comparison between simulated and alumina concentration values, then the absolute relative error at measurement times, and the frequency of feeders and the line current. The model is initialized with measurement and the simulation is started using signals u_2 and i. Every time a new alumina concentration measurement is available, the model is reinitialized to improve the accuracy of the prediction provided by the model.

By analyzing the absolute relative error plot and the inputs, it turns out that the model presents a very good fit for regular operation, when current is not affected by a disturbance or absence of feeding. In particular, the mean absolute relative error is smaller than 1 % for this condition. For the general situation, over the full period of time which is displayed, the model presents an average error of 9.2376%. Therefore, this model should be used for a regular pot operation to estimate the alumina concentration in the collected position.

3.2. Pseudo-Resistance

In equation (28), the parameter identification requires initial knowledge. On wAl_2O_3, which can be available at some specific times but also on ACD,

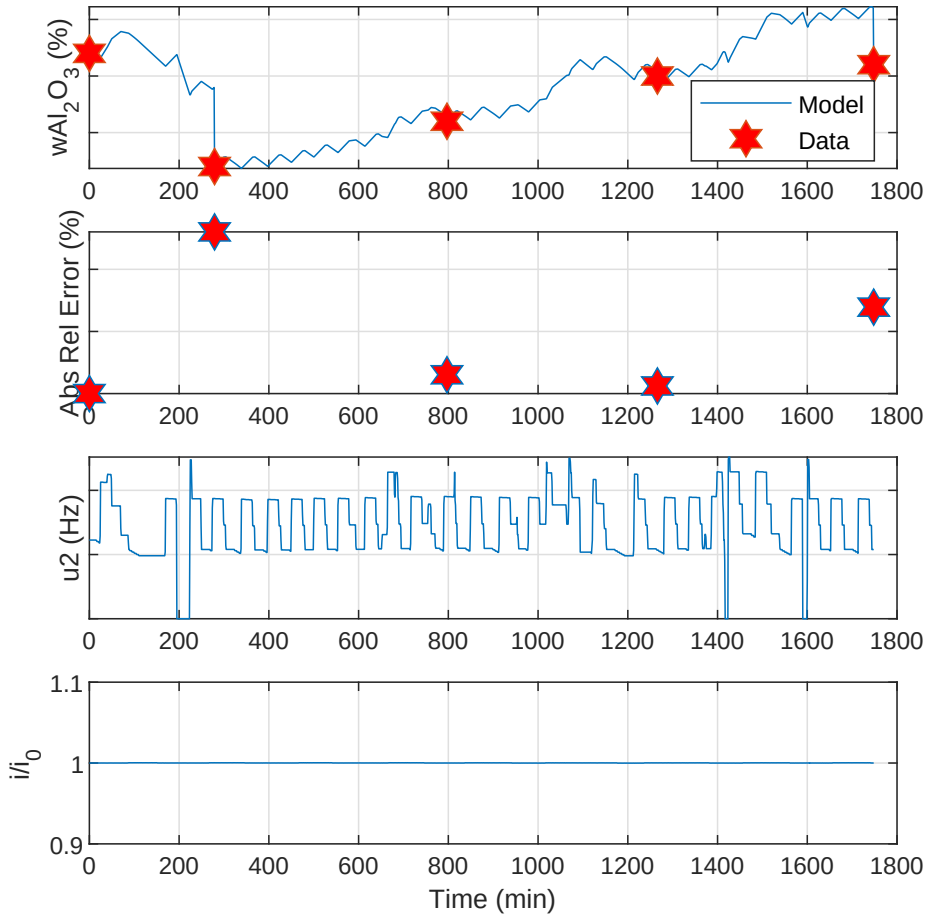

Figure 3: Alumina Concentration Model Validation

which is not measurable during usual operation. One solution is to initialize the procedure at a time when $wAl2O3$ is reliable, and ACD can be inferred from specific physical knowledge, in a similar way as in as [19] for instance. Then, using N samples at times as $\begin{bmatrix}0, & T_s, & \cdots & (N-1)T_s\end{bmatrix}$, it is possible to

organize equation (28) as follows:

$$\begin{bmatrix} \Delta R[1] \\ \vdots \\ \Delta R[N] \end{bmatrix} = \begin{bmatrix} a_{11} & a_{12} & a_{13} & a_{14} \\ \vdots & \vdots & \vdots & \vdots \\ a_{N1} & a_{N2} & a_{N3} & a_{N4} \end{bmatrix} \begin{bmatrix} c \\ d \\ e \\ g \end{bmatrix} \tag{32}$$

where:

$$a_{11} = 2\Delta z_2[0] z_2[0]$$

$$a_{12} = \Delta z_2[0]$$

$$a_{13} = \Delta z_2[0] z_1[0] + \Delta z_1[0] z_2[0]$$

$$a_{14} = \Delta z_1[0]$$

$$\vdots$$

$$a_{N1} = 2\Delta z_2[N-1] \left(z_2[0] + \sum_{k=0}^{N-1} (\alpha_1 u_2[k] - \alpha_2 i[k]) \right)$$

$$a_{N2} = \Delta z_2[N-1]$$

$$a_{N3} = \Delta z_2[N-1] \left(z_1[0] + \sum_{k=0}^{N-1} (u_1[k] + \beta i[k]) \right) + \Delta z_1[N-1] \left(z_2[0] + \sum_{k=0}^{N-1} (\alpha_1 u_2[k] - \alpha_2 i[k]) \right)$$

$$a_{N4} = \Delta z_1[N-1]$$

with notations Δz_1, Δz_2 of equations (29)-(30), and:

$$\Delta R[k] = R[k] - R[k-1] \tag{33}$$

for $k \geq 1$.

155 At this stage, the parameters can be identified using again a least square estimation algorithm. In Figure 4, a comparison between the model output and actual measurements is shown.

The mean absolute error computed for this dataset is 2.21%. However, Figure 4 shows a small drift. This happens because the model (28) is an integrator.
160 Therefore, the difference between the model and the measurements accumulates

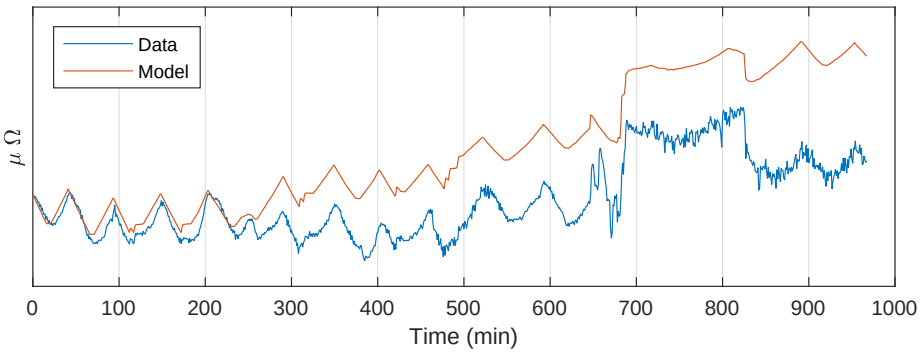

Figure 4: Resistance Model Validation

because of the integrator dynamics. Apart from this, it can be concluded that the proposed estimations are accurate.

4. State Estimation

Based on the models established in Section 2 with the parameter identified in Section 3, the problem of state estimation can now be addressed. Considering the current intensity as a measured disturbance in the system, it is possible to define a discrete-time time varying state-space model of the plant as follows:

$$\begin{cases} \mathbf{x}[n+1] = \underbrace{\begin{bmatrix} 1 & a_{12}[n] & a_{13}[n] \\ 0 & 1 & 0 \\ 0 & 0 & 1 \end{bmatrix}}_{A[n]} \mathbf{x}[n] + \underbrace{\begin{bmatrix} b_1[n] \\ b_2[n] \\ b_3[n] \end{bmatrix}}_{B[n]} \\ y[n] = \underbrace{\begin{bmatrix} 1 & 0 & 0 \end{bmatrix}}_{C} \mathbf{x}[n] \end{cases} \tag{34}$$

where:

$$a_{12}[n] = e(\alpha_1 u_2[n] - \alpha_2 i[n]) \tag{35}$$

$$a_{13}[n] = (2c(\alpha_1 u_2[n] - \alpha_2 i[n]) + e(u_1[n] + \beta i[n]) \tag{36}$$

$$b_1[n] = (d(\alpha_1 u_2[n] - \alpha_2 i[n]) + g(u_1[n] + \beta i[n])) \tag{37}$$

$$b_2[n] = (u_1[n] + \beta i[n]) \tag{38}$$

$$b_3[n] = (\alpha_1 u_2[n] - \alpha_2 i[n]) \tag{39}$$

with all those varying parameters being known quantities and the state vector given by:

$$\mathbf{x}[n] = \begin{bmatrix} R[n] \\ ACD[n] \\ wAl_2O_3[n] \end{bmatrix} \in \mathbb{R}^3 \tag{40}$$

Notice that model (34) is affine in the state. This makes it possible to design an exact linear observer for the nonlinear model by feeding it with measured quantities of equations (35)-(39). To perform this state estimation, a Time-Varying Linear Kalman Filter [20] is used as a state observer. In particular, Kalman Filter equations are given as follows:

Prediction:

$$\hat{\mathbf{x}}[n+1]^- = A[n]\hat{\mathbf{x}}[n] + B[n]$$

$$P[n+1|n] = A[n]P[n|n]A[n]^T + Q_{noise}$$

Update:

$$K[n] = P[n|n-1]C^T(CP[n|n-1]C^T + R_{noise})^{-1}$$

$$\hat{\mathbf{x}}[n] = \hat{\mathbf{x}}[n]^- + K[n](y[k] - C\hat{\mathbf{x}}[n]^-)$$

$$P[n|n] = (I - K[n]C)P[n|n-1]$$

where $\hat{\mathbf{x}}$ is the state estimate vector, P is the covariance matrix, Q_{noise} is the process noise intensity matrix and R_{noise} is the measurement noise matrix. To implement the observer, it is necessary to tune the covariance and noise matrices.

For the considered data, the initial covariance matrix $P[0|0]$ is set to:

$$P[0|0] = \begin{bmatrix} 1 & 0 & 0 \\ 0 & 10^1 & 0 \\ 0 & 0 & 1 \end{bmatrix} \tag{41}$$

The largest entry in the P matrix is related to the ACD [14]. As it is not possible to measure this state, it is given a larger priority. The process and measurement noise matrices, Q_{noise} and R_{noise} respectively are chosen from various trials (as in [14])

$$Q_{noise} = \begin{bmatrix} 10^{-5} & 0 & 0 \\ 0 & 10^{-5} & 0 \\ 0 & 0 & 10^{-5} \end{bmatrix}, \quad R_{noise} = 10^{-5} \tag{42}$$

The proposed observer is tested on data sets with different initial conditions. For each test, a different combination of ACD and wAl_2O_3 initial values is used in a certain operational range, while the values of R are initialized using real measurements. The resulting estimates are shown in Figure 5 with a zoom on initial times in Figure 6. The solid line is the pot resistance measurement, the dashed lines are the states estimates and the "x" markers are the alumina concentration measurements.

From both figures, it is possible to notice a fast convergence, for all estimates regardless of the initial conditions. In addition, Figure 5 also shows the estimates provided by the observer over a long period and compares those with the measurements of wAl_2O_3. The values of the mean absolute error reported in Table 1 confirm the effectiveness of the proposed estimation strategy: good results are indeed achieved jointly for resistance and alumina concentration estimation, while relying on a single model combining their evolution. This validates the overall model and makes the estimation results for ACD (which are consistent with usual industrial knowledge) quite trustable.

5. Conclusions

In this paper, a modeling approach to capture the main dynamics of the Hall-Héroult process has been proposed. In particular, a state affine representation has been obtained, that combines physical-chemical aspects and experimental data. On this basis, a Linear Kalman filter is provided to estimate the states of the system. The model and observer have been validated with experimental data. The proposed observer strategy proved to be reliable in providing accurate estimates of the plant states for unknown initial conditions. The use of these results for monitoring and closed-loop control are part of our ongoing work.

References

[1] K. Grjotheim, B. J. Welch, Aluminium Smelter Technology: A Pure and Applied Approach, Aluminium-Verlag; 2nd edition, 1980.

[2] J. T. Keniry, G. C. Barber, M. P. Taylor, B. J. Welch, Digital processing of anode current signals: an opportunity for improved cell diagnosis and control, Light Metals (2001) 1225–1232.

[3] P. Côté, O. Martin, B. Allano, V. Dassylva-Raymond, Predicting instability and current efficiency of industrial cells, in: Light Metals 2017, Springer, 2017, pp. 623–629.

[4] M. Dupuis, V. Bojarevics, Demo retrofit study of a chinese inspired cell technology, in: Light Metals 2020, Springer, 2020, pp. 495–509.

[5] D. S. Wong, G. Matthews, A. T. Tabereaux, T. Buckley, M. M. Dorreen,

Table 1: Estimations Final Values Comparison

	Mean Absolute Relative Error
R	0.07%
wAl_2O_3	4.19 %

The australian energy crisis, its impact on domestic aluminium smelting and potential solutions, in: Light Metals 2020, Springer, 2020, pp. 791–802.

[6] S. R. Jakobsen, K. Hestetun, M. Hovd, I. Solberg, Estimating alumina concentration distribution in aluminium electrolysis cells, IFAC Proceedings Volumes 34 (18) (2001) 303–308.

[7] Y. Yao, C.-Y. Cheung, J. Bao, M. Skyllas-Kazacos, B. J. Welch, S. Akhmetov, Estimation of spatial alumina concentration in an aluminum reduction cell using a multilevel state observer, AIChE Journal 63 (7) (2017) 2806–2818.

[8] G. P. Bearne, The development of aluminum reduction cell process control, JOM 51 (5) (1999) 16–22.

[9] P. Biedler, Modeling of an aluminum reduction cell for the development of a state estimator, Ph.D. thesis, West Virginia University (2003).

[10] P. Homsi, J.-M. Peyneau, M. Reverdy, Overview of process control in reduction cells and potlines, in: Essential Readings in Light Metals, Springer, 2016, pp. 739–746.

[11] S. Kolås, B. Foss, T. S. Schei, State estimation is the real challenge in NMPC, in: International workshop on assessment and future directions of nonlinear model predictive control, Pavia, Italy, 2008.

[12] K. Hestetun, M. Hovd, Detecting abnormal feed rate in aluminium electrolysis using extended Kalman filter, IFAC Proceedings Volumes 38 (1) (2005) 85–90.

[13] J. B. Moore, B. Anderson, Optimal filtering, Prentice-Hall, 1979.

[14] L. J. da Silva Moreira, G. Besançon, F. Ferrante, M. Fiacchini, H. Roustan, Model based approach for online monitoring of aluminum production process, in: Light Metals 2020, Springer, 2020, pp. 566–571.

[15] L. J. da Silva Moreira, M. Fiacchini, G. Besançon, F. Ferrante, H. Roustan, State affine modeling and observer design for Hall-Héroult process, in: IFAC World Congress 2020, 2020.

[16] A. Ţiclea, G. Besançon, Exponential forgetting factor observer in discrete time, Systems & Control Letters 62 (9) (2013) 756–763.

[17] S.-q. Zhan, L. Mao, J.-m. Zhou, J.-h. Yang, Y.-w. Zhou, Analysis and modeling of alumina dissolution based on heat and mass transfer, Transactions of nonferrous metals society of China 25 (5) (2015) 1648–1656.

[18] C. G. Zoski, Handbook of electrochemistry, Elsevier, 2006.

[19] W. Haupin, Interpreting the components of cell voltage, in: Essential Readings in Light Metals, Springer, 2016, pp. 153–159.

[20] R. E. Kalman, A new approach to linear filtering and prediction problems, Journal of basic Engineering 82 (1) (1960) 35–45.

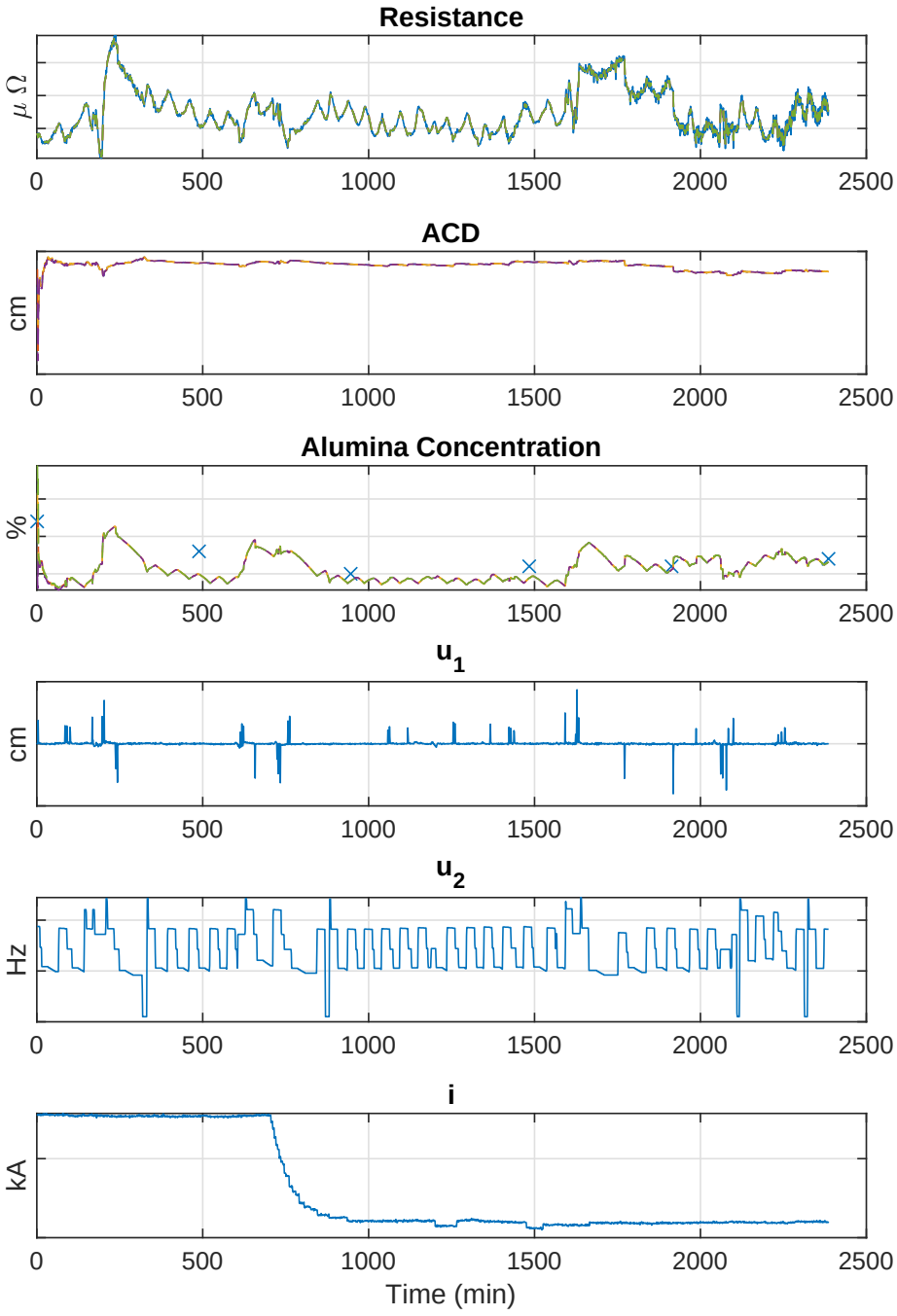

Figure 5: State Estimation for a long period - Each dashed line is a state estimation with different initial condition and the solid line is the measurement.

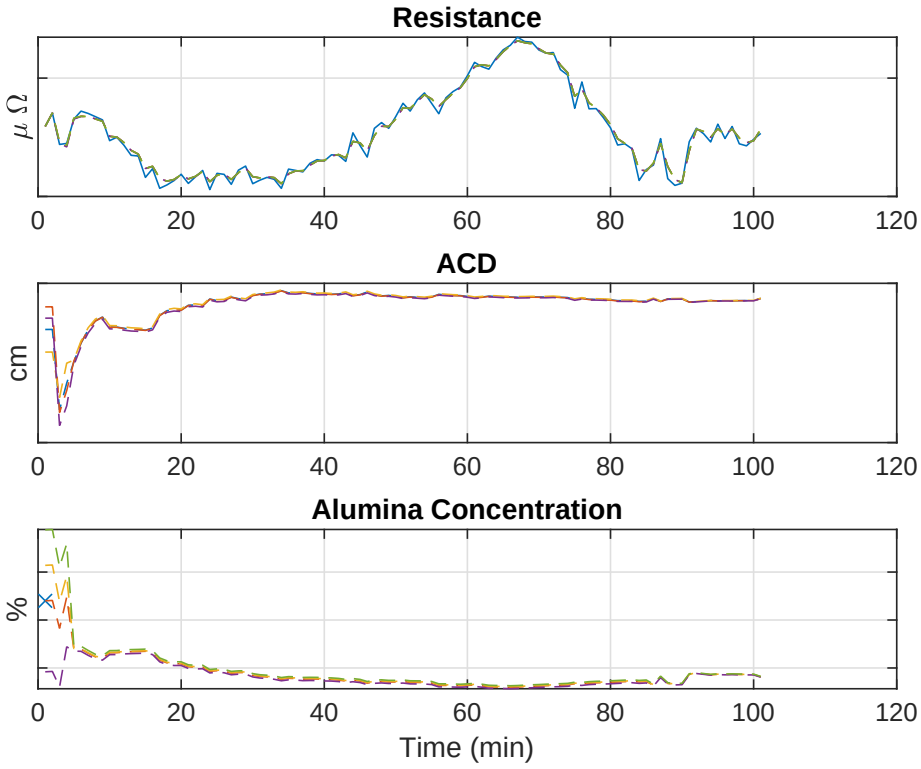

Figure 6: State Estimation for a short period - Each dashed line is a state estimation with different initial condition and the solid line is the measurement.